

First-principles study of the electronic and magnetic structures of the tetragonal and orthorhombic phases of $\text{Ca}_3\text{Mn}_2\text{O}_7$

S. F. Matar,^{1,*} V. Eyert,² A. Villesuzanne,¹ and M.-H. Whangbo³

¹ICMCB, CNRS, Université Bordeaux I, 87 Avenue Docteur Albert Schweitzer, 33608 Pessac Cedex, France

²Institut für Physik, Universität Augsburg, 86135 Augsburg, Germany

³Department of Chemistry, North Carolina State University, Raleigh, North Carolina 27695, USA

(Received 7 November 2006; revised manuscript received 21 March 2007; published 3 August 2007)

On the basis of density functional theory electronic band structure calculations using the augmented spherical wave method, the electronic and magnetic properties of the orthorhombic and tetragonal phases of $\text{Ca}_3\text{Mn}_2\text{O}_7$ were investigated and the spin exchange interactions of the orthorhombic phase were analyzed. Our calculations show that the magnetic insulating states are more stable than the nonmagnetic metallic state for both polymorphs of $\text{Ca}_3\text{Mn}_2\text{O}_7$, the orthorhombic phase is more stable than the tetragonal phase, and the ground state of the orthorhombic phase is antiferromagnetic. The total energies calculated for the three spin states of the orthorhombic phase of $\text{Ca}_3\text{Mn}_2\text{O}_7$ led to estimates of the spin exchange interactions $J_{nn} = -3.36$ meV and $J_{nnn} = -0.06$ meV. The accuracy of these estimates was tested by calculating the Curie-Weiss temperature within the mean-field approximation.

DOI: [10.1103/PhysRevB.76.054403](https://doi.org/10.1103/PhysRevB.76.054403)

PACS number(s): 75.47.Lx, 75.30.Et, 73.20.At, 71.15.Mb

I. INTRODUCTION

Due to their potential technological application, magnetic ternary manganese oxides have received much attention in the past decade.^{1–3} It is an important theoretical issue to understand their electronic and magnetic properties.^{4,5} In accounting for such properties of magnetic oxides, density functional theory (DFT)^{6,7} electronic structure calculations using the local spin density approximation (LSDA)⁸ and the generalized gradient approximation (GGA)⁹ have proven very reliable. Reduced dimensionality perovskite based systems are found in the Ruddlesden-Popper (RP) family: $\text{Ca}_{n+1}\text{Mn}_n\text{O}_{3n+1}$.¹⁰ The diamagnetic CaO rocksalt layers alternate with the magnetic $(\text{CaMnO}_3)_n$ layers along the crystallographic c direction, where n represents the number of MnO_3 perovskite sheets in each $(\text{CaMnO}_3)_n$ layer. To emphasize this structural feature, the formulas for these oxides can be rewritten as $(\text{CaO})(\text{CaMnO}_3)_n$ with $n=1, 2, 3, \dots, \infty$. Known examples of this RP family are Ca_2MnO_4 ($n=1$), $\text{Ca}_3\text{Mn}_2\text{O}_7$ ($n=2$), and $\text{Ca}_4\text{Mn}_3\text{O}_{10}$ ($n=3$).¹¹ Note that the $n=\infty$ member is simply the perovskite CaMnO_3 .^{12,13} In a recent electronic structure study,¹⁴ it was shown that the $n=1$ RP member, Ca_2MnO_4 , and its reduced phase $\text{Ca}_2\text{MnO}_{3.5}$ are antiferromagnetic (AF) insulators with band gap of ~ 1 eV. According to a neutron diffraction study at room temperature,¹⁵ the $n=2$ RP member, $\text{Ca}_3\text{Mn}_2\text{O}_7$, exists as a mixture of the majority orthorhombic and the minority tetragonal phases. The main structural difference between the two systems is depicted in Fig. 1. Due to the tilting of the MnO_6 octahedra, the Mn-O-Mn angles between two adjacent corner-sharing octahedra are considerably smaller than 180° (i.e., 159.1° , 163.2° , and 163.9°). $\text{Ca}_3\text{Mn}_2\text{O}_7$ undergoes a three-dimensional magnetic ordering below $T_N \sim 110\text{--}115$ K with a G -type AF structure. In view of this coexistence of phases, which is an unusual feature in such reduced dimensionality manganese oxide systems, it is relevant to assess differences between the two crystal structures in terms of the electronic structure description. In the present

work, the two polymorphs of $\text{Ca}_3\text{Mn}_2\text{O}_7$ are examined with first principles DFT calculations.

II. CALCULATIONS

Our DFT calculations employed the all-electron augmented spherical wave (ASW) method in its scalar-

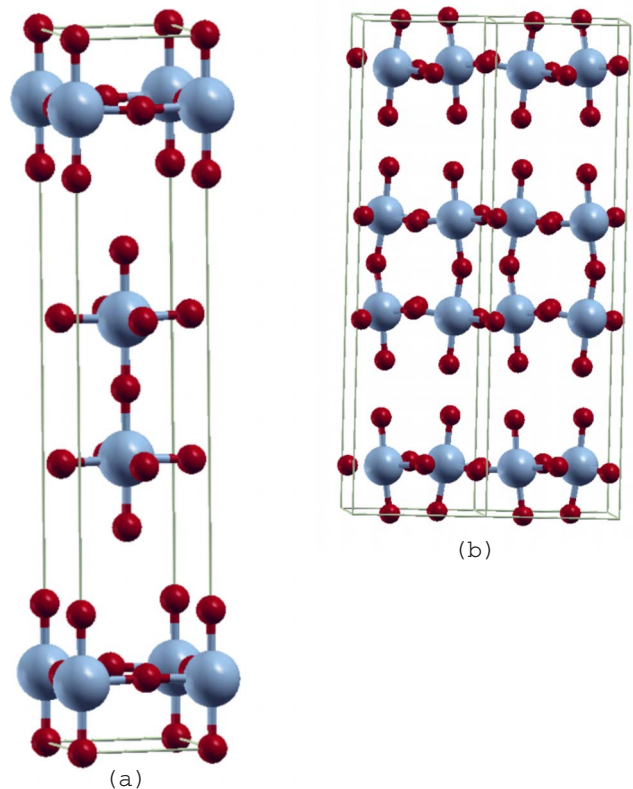


FIG. 1. (Color online) Sketches of the structures of the (a) minority tetragonal and (b) majority orthorhombic phases of $\text{Ca}_3\text{Mn}_2\text{O}_7$. Large and small spheres point to Mn and O atoms. Calcium atoms are not shown.

relativistic implementation.^{16,17} As preliminary calculations revealed that the GGA describes the effects of exchange and correlation better than the LSDA, hence leading to a more accurate description of the energy differences between different ordered magnetic states, we opted for a use of the GGA in the form proposed by Perdew *et al.*⁹ In the ASW method, the wave function is expanded in atom-centered augmented spherical waves, which are Hankel functions and numerical solutions of Schrödinger's equation, respectively, outside and inside the so-called augmentation spheres. In order to optimize the basis set, additional augmented spherical waves were placed at carefully selected interstitial sites. The choice of these sites as well as the augmentation radii were automatically determined using the sphere-geometry optimization algorithm.¹⁸ The Ca $4s$, Mn $4s$, Mn $3d$, and O $2p$ states were treated as valence states, and the low-lying O $2s$ states as core states. The basis set was complemented by wave functions of s , p , and possibly d symmetries centered at the interstitial sites. A sufficiently large number of k points was used to sample the irreducible wedge of the Brillouin zone, and the energy and charge differences between successive iterations were converged below $\Delta E=10^{-8}$ Ry and $\Delta Q=10^{-8}$, respectively, to obtain accurate values of the magnetic moments and accurate total energy differences between various ordered magnetic states. To extract more information about the nature of the interactions between the atomic constituents from electronic structure calculations, the crystal orbital overlap population (COOP)¹⁹ or the crystal orbital Hamiltonian population (COHP)²⁰ may be employed. Both approaches provide a qualitative description of the bonding, nonbonding, and antibonding interactions between two atoms. A slight refinement of the COHP was recently proposed in the form of the "energy of covalent bond" (ECOV), which combines COHP and COOP to calculate quantities independent of the choice of the zero of potential.²¹ Both COOP and ECOV give similar general trends, but COOP, when defined within plane-wave basis sets, exaggerates the magnitude of antibonding states. In the present work, the ECOV was used for the chemical bonding analysis. It is noted that negative, positive, and zero values of ECOV are associated with bonding, antibonding, and nonbonding interactions, respectively.

III. RESULTS AND DISCUSSION

A. Nonmagnetic configuration

To gain insight into the chemical bonding in the two forms of $\text{Ca}_3\text{Mn}_2\text{O}_7$, their nonmagnetic (NM) states were calculated by performing non-spin-polarized electronic structure calculations by enforcing spin degeneracy for all species. Our calculations show charge transfer from the cation sites (Ca^{2+} , Mn^{4+}) to the anionic sites of oxygen as well as toward the voids, but the amount of charge transfer is not significant of an ionic character of the atomic constituents. The plots of the projected density of states (DOS) for the constituent atom sites are presented in Fig. 2. The projected DOS plots calculated for the five Mn $3d$ orbitals are presented in Fig. 3, and the ECOV plots calculated for the various Mn-O bonds in Fig. 4.

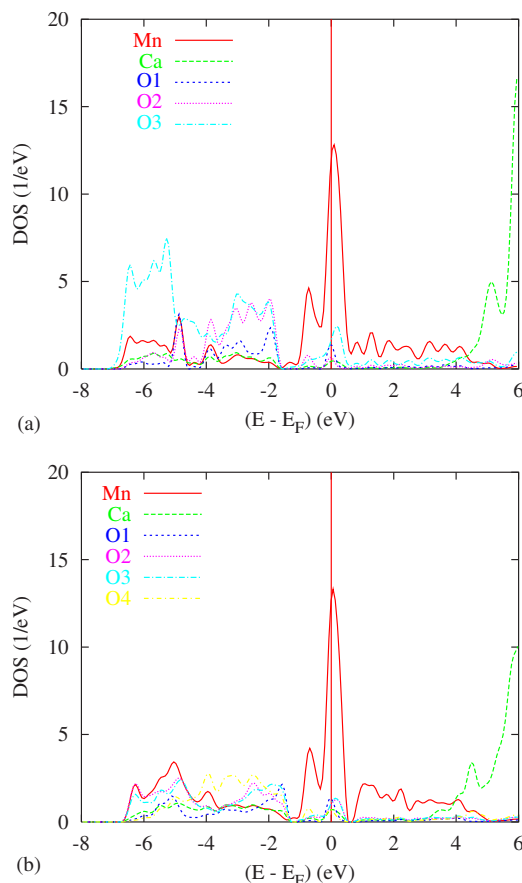


FIG. 2. (Color online) Projected DOS plots of the atomic sites calculated for the NM states of the (a) minority tetragonal and (b) majority orthorhombic phases of $\text{Ca}_3\text{Mn}_2\text{O}_7$.

The comparison of Figs. 2 and 4 shows that the valence bands (VB's) are dominated by Mn-O bonding. The Mn-O interactions are bonding in the major part of the VB's with strong contributions in the $-8, -6$ eV region (Fig. 2), i.e., where the Mn e_g orbitals (Fig. 3) make σ bonding with the O $2p$ orbitals. The s -like Ca states are smeared into the whole range of the VB's (Fig. 2). For both polymorphs of $\text{Ca}_3\text{Mn}_2\text{O}_7$, the Fermi level E_F occurs near the DOS peak dominated by the Mn $3d$ states so that the DOS value at the Fermi level, $n(E_F)$, is large. The DOS peak around E_F arises from the t_{2g} -block bands in which the Mn t_{2g} orbitals make weak π -antibonding interactions with the O $2p$ orbitals. The existence of Mn-O antibonding states in this DOS peak is clearly seen from the ECOV plot (Fig. 4).

The occurrence of the Fermi level around a sharp DOS peak with a large $n(E_F)$ value indicates an instability toward spin polarization. This can be inferred from Stoner's theory analysis (see Ref. 22 for a review on magnetic oxides). Within the Stoner theory, the large DOS at the Fermi level is related to the instability of the nonmagnetic state with respect to the onset of intraband spin polarization when $n(E_F)I > 1$. In this so-called Stoner criterion I is the Stoner integral calculated and tabulated by Janak⁸ for the elemental systems: $I(\text{Mn})=0.408$ eV. With $n_{\text{Mn}}(E_F)=8.5$ eV^{-1} , the $n(E_F)I$ value of 3.47 clearly points to an unstable non mag-

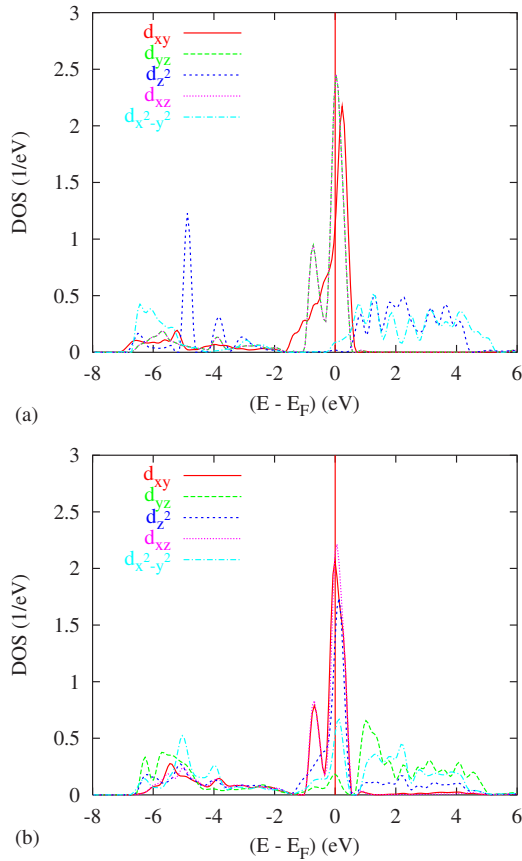


FIG. 3. (Color online) Projected DOS plots of the Mn $3d$ orbitals calculated for the NM states of the (a) minority tetragonal and (b) majority orthorhombic phases of $\text{Ca}_3\text{Mn}_2\text{O}_7$.

netic state so that a nonzero magnetic moment on the Mn sites should occur when two spin populations are accounted for in the calculations.

B. Magnetic states

Spin-polarized electronic structure calculations were carried out for the ferromagnetic (FM) state of the orthorhombic and tetragonal phases of $\text{Ca}_3\text{Mn}_2\text{O}_7$, and for the AF state of the orthorhombic phase of $\text{Ca}_3\text{Mn}_2\text{O}_7$. There are a number of possible AF spin arrangements. Although experimental findings¹⁵ point to a G -type AF arrangement, in the present study, we considered two types of AF orderings for the sake of establishing comparisons and for testing the theory against the experiment, i.e., the G - and A -type AF states shown in Fig. 5. In the G -type AF state, the antiferromagnetically ordered planes of Mn sites are antiferromagnetically coupled. In the A -type AF arrangement, the ferromagnetically ordered planes of Mn sites are antiferromagnetically coupled within each perovskite layer.

Results of our calculations for the FM state of the tetragonal and orthorhombic phases of $\text{Ca}_3\text{Mn}_2\text{O}_7$ are summarized in Table I as well as in Fig. 6. For both phases, the FM state is substantially more stable than the NM states (i.e., $E_{FM} < E_{NM}$), and the total moment per f.u. is $6.0\mu_B$ (Table I), as expected for the high-spin $\text{Mn}^{4+}(d^3)$ ions in $\text{Ca}_3\text{Mn}_2\text{O}_7$. The

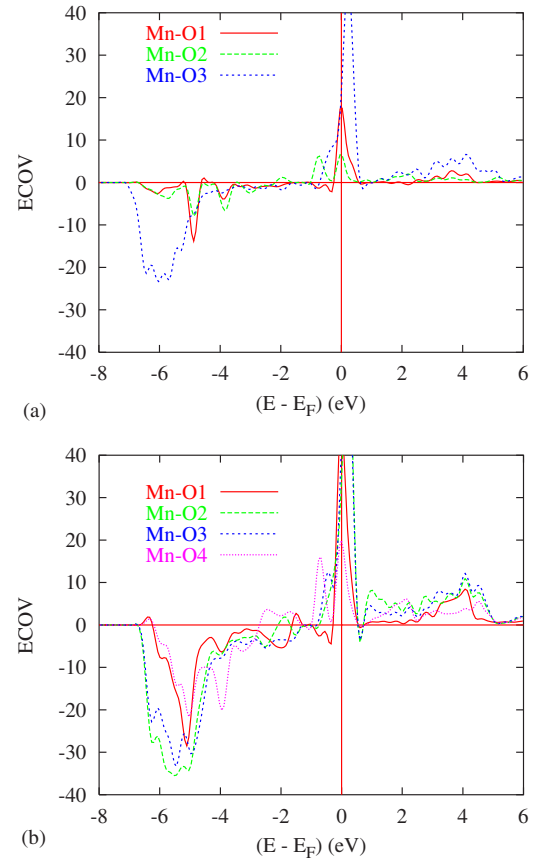


FIG. 4. (Color online) ECOV plots of the Mn-O bonds calculated for the NM states of the (a) minority tetragonal and (b) majority orthorhombic phases of $\text{Ca}_3\text{Mn}_2\text{O}_7$.

total energy obtained for the orthorhombic phase is by 170 meV/f.u. lower than that of the tetragonal phase, which is consistent with the finding that the orthorhombic and tetragonal phases are the majority and minority phases, respectively. The projected DOS plots calculated for the FM state of the orthorhombic $\text{Ca}_3\text{Mn}_2\text{O}_7$ are presented in Fig. 6(a). The up-spin and down-spin bands are strongly splitted such that the up-spin t_{2g} -block bands are completely filled, while the down-spin t_{2g} -block bands are empty, as expected for the high-spin $\text{Mn}^{4+}(d^3)$ ions. The down- and up-spin bands have band gaps of about 1.0 and 0.3 eV, respectively. Given the fact that both the LSDA and the GGA underestimate band gaps, the FM state of $\text{Ca}_3\text{Mn}_2\text{O}_7$ should be insulating experimentally. However, the FM state is not the magnetic ground state of $\text{Ca}_3\text{Mn}_2\text{O}_7$, as will be discussed in the next section. Figure 6(b) shows the ECOV plots for the Mn-O bonds calculated for the up-spin and down-spin bands of the orthorhombic phase. The VB's exhibit Mn-O bonding interactions up to -2 eV in both up-spin and down-spin bands. The energy region between -2 eV and the Fermi level shows Mn-O antibonding interactions due to the π -type antibonding interactions of the t_{2g} -block bands in the up-spin bands, but this feature is missing in the down-spin bands because the down-spin t_{2g} -block bands are raised above the Fermi level. Thus, the exchange splitting in the FM state enhances Mn-O bonding interactions in $\text{Ca}_3\text{Mn}_2\text{O}_7$.

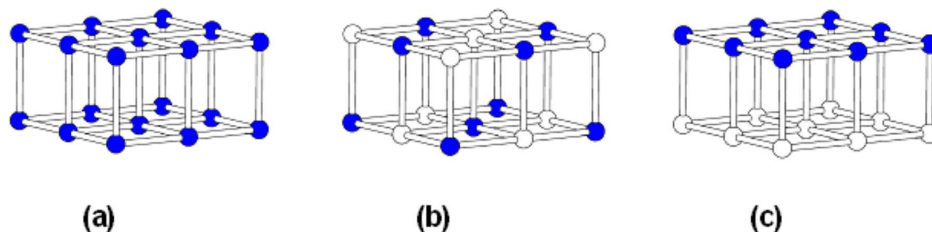


FIG. 5. (Color online) Schematic representations of the Mn spin arrangements in the (a) FM, (b) the *G*-type AF, and (c) *A*-type AF states of $\text{Ca}_3\text{Mn}_2\text{O}_7$. Dark (blue) and white (open) spheres refer to up- and down-spin alignments, respectively.

Results of calculations for the *G*- and *A*-type AF states of the orthorhombic phase of $\text{Ca}_3\text{Mn}_2\text{O}_7$ are summarized in Table II and Fig. 7. Both AF states are more stable than the FM state, and the *G*-type AF state is slightly more stable than the *A*-type AF state (Table II). The latter is consistent with the neutron diffraction study,¹³ which found a *G*-type AF ordering for $\text{Ca}_3\text{Mn}_2\text{O}_7$. While the resulting magnetization is zero as expected in AF order, the atomic magnetic moments and the resulting up-spin and down-spin sublattice magnetizations are reduced with respect to their value in the ferromagnetic configuration.

The DOS and band structure are shown in Fig. 7 for one magnetic sublattice. The similarities with the features observed in Fig. 6 for the ferromagnetic case are present here too. So at least from the point of view of the electronic band structure, some relationship is persistent, although the AF state is the ground state with an insulating character. Furthermore, the large dispersion of the bands within the CB [Fig. 7(b)] illustrates the itinerant character of the e_g states. The gap of ~ 0.4 eV, whose experimental magnitude is not known, is found direct, between Γ_V and Γ_C . Since both the LSDA and the GGA underestimate the band gap, the system can be expected to be insulating experimentally.

IV. ANALYSIS OF THE SPIN EXCHANGE INTERACTIONS

It is of interest to estimate the nearest-neighbor (nn) spin exchange J_{nn} and the next-nearest-neighbor (nnn) spin ex-

TABLE I. Total energies and magnetic moments of the atomic sites calculated for the ferromagnetic states of the tetragonal and orthorhombic phases of $\text{Ca}_3\text{Mn}_2\text{O}_7$. The energies are given in units of eV per half the f.u. (i.e., per Mn) with respect to those of the non-spin-polarized state. The magnetic moments are given in units of Bohr magneton (μ_B).

Parameters	Tetragonal	Orthorhombic
ΔE_{FM-NM} (eV)	-1.442	-1.610
ΔE_{FM-NM} (eV)/Mn	-0.721	-0.831
$\mu(\text{Mn})$	2.729	2.719
$\mu(\text{O1})$	0.088	0.092
$\mu(\text{O2})$	-0.001	0.047
$\mu(\text{O3})$	0.073	0.056
$\mu(\text{O4})$		0.014
$\mu(\text{f.u.})$	6.0	6.0

change J_{nnn} interactions of the $(\text{CaMnO}_3)_2$ double-perovskite layer in the orthorhombic phase of $\text{Ca}_3\text{Mn}_2\text{O}_7$. The spin exchange interactions between the adjacent double-perovskite layers are expected to be negligible, so we consider only those interactions within a double-perovskite layer. Then, each Mn site has five nn and eight nnn spin exchange interactions. For simplicity, we assume that all five nn interactions are identical, and so are all the eight nnn interactions. Consequently, in terms of J_{nn} and J_{nnn} , the energies per Mn site of the FM, *G*-type AF, and *A*-type AF states are written as shown in Eq. (1),²³⁻²⁵ where N is the number of unpaired spins at each Mn^{4+} site (i.e., $N=3$). Just like the analysis done for the similar Sr based layered system,⁴ the J values of

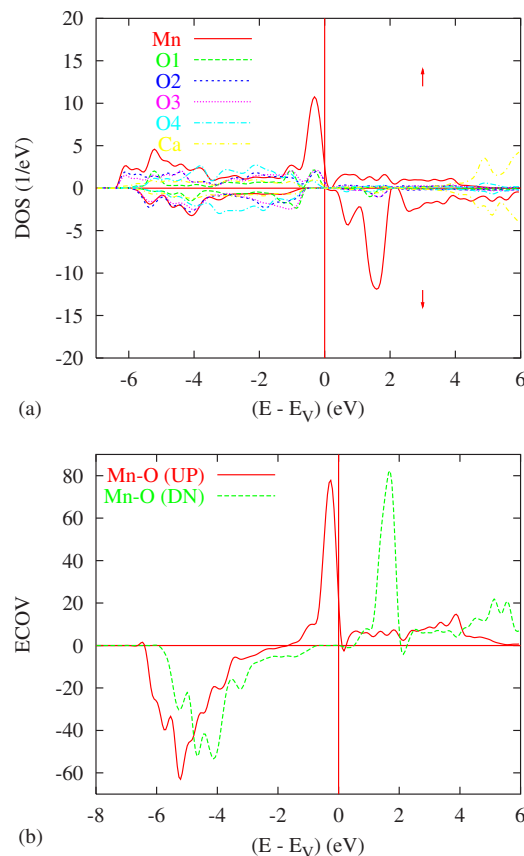


FIG. 6. (Color online) FM $\text{Ca}_3\text{Mn}_2\text{O}_7$. (a) Site and spin projected DOS and (b) chemical bonding (ECOV) for Mn-O interaction regrouping all four oxygen sublattices. Energy reference is with respect to the VB top E_V due to the closely insulating character.

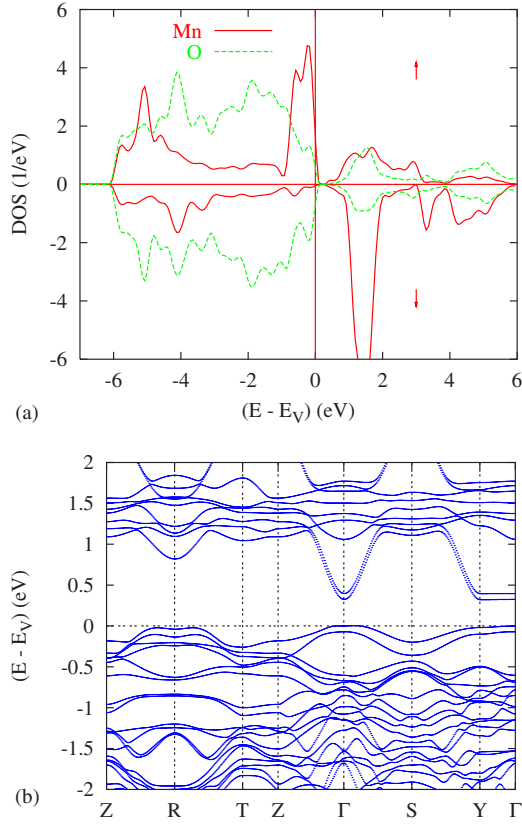


FIG. 7. (Color online) AF $\text{Ca}_3\text{Mn}_2\text{O}_7$: (a) Site and spin projected DOS and (b) band structure. Plots are for one magnetic sublattice. O-PDOS regroup all oxygen sites.

our system are not known experimentally to the best of our knowledge. Thus, the calculation of J_{nn} and J_{nnn} was carried out.

$$E(\text{FM}) = \frac{1}{2}(-5J_{nn} - 8J_{nnn})\left(\frac{N^2}{4}\right) = \left(\frac{N^2}{4}\right)(-2.5J_{nn} - 4J_{nnn}),$$

$$E(G - \text{AF}) = \frac{1}{2}(5J_{nn} - 8J_{nnn})\left(\frac{N^2}{4}\right) = \left(\frac{N^2}{4}\right)(2.5J_{nn} - 4J_{nnn}),$$

$$E(A - \text{AF}) = \frac{1}{2}(-3J_{nn})\left(\frac{N^2}{4}\right) = \left(\frac{N^2}{4}\right)(-1.5J_{nn}). \quad (1)$$

According to the results of our electronic band structure calculations (Table II), we have

$$E(\text{FM}) - E(G - \text{AF}) = 37.8 \text{ meV/Mn},$$

$$E(A - \text{AF}) - E(G - \text{AF}) = 29.7 \text{ meV/Mn}. \quad (2)$$

From Eqs. (1) and (2), it is estimated that $J_{nn} = -3.36 \text{ meV}$ and $J_{nnn} = -0.06 \text{ meV}$, i.e., $J_{nn}/k_B = -39 \text{ K}$ and $J_{nnn}/k_B = -0.7 \text{ K}$, where k_B is the Boltzmann constant. The nn interaction is strongly AF, and the nnn interaction is very weakly AF. Therefore, within the mean-field approximation, the

TABLE II. Total energies and magnetic moments of the atomic sites calculated for the A- and G-type antiferromagnetic states of the orthorhombic phases of $\text{Ca}_3\text{Mn}_2\text{O}_7$. The energies are given in units of eV per half the f.u. (i.e., per Mn) with respect to those of the FM state. The magnetic moments are given in units of Bohr magneton (μ_B).

Parameters	A-type AF	G-type AF
ΔE_{AF-FM} (eV)	-0.0082	-0.0378
$\mu(\text{Mn})$	± 2.613	± 2.678
$\mu(\text{O1})$	± 0.058	~ 0.0
$\mu(\text{O2})$	0.0	± 0.03
$\mu(\text{O3})$	0.0	± 0.05
$\mu(\text{O4})$	0.0	0.02
$\mu(\text{f.u.})$	± 5.168	± 5.380

Curie-Weiss temperature of $\text{Ca}_3\text{Mn}_2\text{O}_7$ can be estimated from the J_{nn} value according to the expression

$$\Theta = \frac{zJ_{nn}S(S+1)}{3k_B}, \quad (3)$$

where $z=5$ and $S=\frac{3}{2}$ for the high-spin Mn^{3+} . For $J_{nn}/k_B \sim -39 \text{ K}$, we obtain $\Theta = -244 \text{ K}$, which is somewhat smaller in magnitude than the experimental value $\Theta_{\text{expt}} = -465 \text{ K}$.²⁶ This suggests that our calculations underestimated the spin exchange interactions of $\text{Ca}_3\text{Mn}_2\text{O}_7$ by a factor of approximately 2. Under the approximation of the DFT and its functionals, such a discrepancy can be expected when comparisons are made with mean-field analysis results. In general, however, spin exchange interactions are frequently overestimated when the energy differences from DFT calculations are mapped onto those from an Ising spin Hamiltonian.^{23,27-32}

V. CONCLUSION

Our electronic structure study reveals that for both polymorphs of $\text{Ca}_3\text{Mn}_2\text{O}_7$, the magnetic states are more stable than the nonmagnetic states. The spin polarization makes $\text{Ca}_3\text{Mn}_2\text{O}_7$ insulating and lowers its energy mainly through exchange, leading to a magnetic moment on Mn expected for a high-spin Mn^{4+} (d^3) ion. In the spin-polarized configuration the down-spin states provide more Mn-O bonding than do the up-spin states because the down-spin Mn t_{2g} -block bands are raised above the Fermi level. In agreement with the experiment, our calculations show that the orthorhombic phase is more stable than the tetragonal phase, and the ground state of the orthorhombic phase is G-type AF. The total energies of the FM, A-type AF, and G-type AF states of $\text{Ca}_3\text{Mn}_2\text{O}_7$ obtained from our calculations lead to the estimates of the spin exchange interactions $J_{nn}/k_B \sim -39 \text{ K}$ and $J_{nnn}/k_B \sim -0.7 \text{ K}$. The Curie-Weiss temperature Θ estimated from these spin exchange parameters is approximately half the experimental value, so that our calculations underestimated the values of the spin exchange parameters by a factor of approximately 2.

ACKNOWLEDGMENTS

We acknowledge support from the computational facilities provided by the computer center of the University Bordeaux 1 within the *M3PEC* (<http://www.m3pec.u-bordeaux1.fr>) intensive calculations project partly financed

by the Conseil Régional d'Aquitaine. M.-H.W. thanks the support by the Office of Basic Energy Sciences, Division of Materials Sciences, U.S. Department of Energy, under Grant No. DE-FG02-86ER45259. V.E. acknowledges support by the Deutsche Forschungsgemeinschaft through SFB 484.

*Corresponding author. s.matar@u-bordeaux1.fr

- ¹M. A. Subramanian, A. P. Ramirez, and G. H. Kwei, *Solid State Ionics* **108**, 185 (1998).
- ²B. Vertruyen, D. Flahaut, S. Hébert, A. Maignan, C. Martin, M. Hervieu, and B. Raveau, *J. Magn. Magn. Mater.* **280**, 75 (2004).
- ³H. Park, E. Vescovo, H. J. Kim, C. Kwon, R. Ramesh, and T. Venkatesan, *Nature (London)* **392**, 794 (1998).
- ⁴H. Meskine, Z. S. Popovic, and S. Satpathy, *Phys. Rev. B* **65**, 094402 (2002).
- ⁵P. K. de Boer and R. A. de Groot, *Phys. Rev. B* **60**, 10758 (1999).
- ⁶P. Hohenberg and W. Kohn, *Phys. Rev.* **136**, B864 (1964).
- ⁷W. Kohn and L. J. Sham, *Phys. Rev.* **140**, A1133 (1965).
- ⁸J. F. Janak, *Solid State Commun.* **25**, 53 (1978).
- ⁹J. P. Perdew, K. Burke, and M. Ernzerhof, *Phys. Rev. Lett.* **77**, 3865 (1996).
- ¹⁰S. N. Ruddlesden and P. Popper, *Acta Crystallogr.* **10**, 538 (1957).
- ¹¹J. B. MacChesney, H. J. Williams, J. F. Potter, and R. Sherwood, *Phys. Rev.* **164**, 779 (1967).
- ¹²K. R. Poeppelmeier, M. E. Leonowicz, J. C. Scanlon, J. M. Longo, and W. B. Yelon, *J. Solid State Chem.* **45**, 71 (1982).
- ¹³S. F. Matar, F. Studer, B. Siberchicot, M. A. Subramanian, G. Demazeau, and J. Etourneau, *Eur. Phys. J.: Appl. Phys.* **4**, 143 (1998).
- ¹⁴S. F. Matar, M. A. Subramanian, and R. Wehrich, *Chem. Phys.* **310**, 231 (2005).
- ¹⁵M. V. Lobanov, M. Greenblatt, E. N. Caspi, J. D. Jorgensen, D. V. Sheptyakov, B. H. Toby, C. E. Botez, and P. W. Stephens, *J. Phys.: Condens. Matter* **16**, 5339 (2004).
- ¹⁶A. R. Williams, J. Kübler, and C. D. Gelatt, *Phys. Rev. B* **19**, 6094 (1979).
- ¹⁷V. Eyert, *The Augmented Spherical Wave Method: A Comprehensive Treatment*, Lecture Notes in Physics Vol. 719 (Springer, Heidelberg, 2007).
- ¹⁸V. Eyert and K.-H. Höck, *Phys. Rev. B* **57**, 12727 (1998).
- ¹⁹R. Hoffmann, *Angew. Chem., Int. Ed. Engl.* **26**, 846 (1987).
- ²⁰R. Dronskowski and P. E. Blöchl, *J. Phys. Chem.* **97**, 8617 (1993).
- ²¹G. Bester and M. Fahnle, *J. Phys.: Condens. Matter* **13**, 11541 (2001); **13**, 11551 (2001).
- ²²S. F. Matar, *Prog. Solid State Chem.* **31**, 239 (2003).
- ²³D. Dai and M.-H. Whangbo, *J. Chem. Phys.* **114**, 2887 (2001).
- ²⁴D. Dai, M.-H. Whangbo, H.-J. Koo, X. Rocquefelte, S. Jobic, and A. Villesuzanne, *Inorg. Chem.* **44**, 2407 (2005).
- ²⁵D. Dai, M.-H. Whangbo, J. Köhler, C. Hoch, and A. Villesuzanne, *Chem. Mater.* **18**, 3281 (2006).
- ²⁶I. D. Fawcett, E. Kim, M. Greenblatt, M. Croft, and L. A. Bendersky, *Phys. Rev. B* **62**, 6485 (2000).
- ²⁷D. Dai and M.-H. Whangbo, *J. Chem. Phys.* **114**, 2887 (2001).
- ²⁸D. Ködderitzsch, W. Hergert, W. M. Temmerman, Z. Szotek, A. Ernst, and H. Winter, *Phys. Rev. B* **66**, 064434 (2002).
- ²⁹D. Dai, H.-J. Koo, and M.-H. Whangbo, *J. Solid State Chem.* **175**, 341 (2003).
- ³⁰R. Grau-Crespo, N. H. de Leeuw, and C. R. Catlow, *J. Mater. Chem.* **13**, 2848 (2003).
- ³¹N. Lampis, C. Franchini, G. Satta, A. Geddo-Lehmann, and S. Massidda, *Phys. Rev. B* **69**, 064412 (2004).
- ³²H. Ben Yahia, E. Gaudin, J. Darriet, M. Banks, R. K. Kremer, A. Villesuzanne, and M.-H. Whangbo, *Inorg. Chem.* **44**, 3087 (2005).